

Analyses of Transformation Kinetics of Carbide-Free Bainite Above and Below the Athermal Martensite-Start Temperature

I.A. YAKUBTSOV and G.R. PURDY

The isothermal transformation kinetics of austenite decomposition in Fe-0.4C-2.78Mn-1.81Si was analyzed by an electrical resistivity technique in the temperature interval 723 K to 418 K (450 °C to 145 °C). The analysis of transformation kinetics of the bainite transformation was performed using the Johnson–Mehl–Avrami–Kolgomorov (JMAK) and Austin–Rickett (AR) approaches. The kinetic parameters, the reaction constant n , rate constant $k = k(T)$, and apparent activation energy Q were evaluated for isothermal transformations below and above the martensite-start temperature $M_S = 548$ K (275 °C), which was determined experimentally. The formation of strain-induced martensite, which starts to accompany the bainite transformation at just above M_S , increases the rate of transformation and decreases the apparent activation energy of austenite decomposition.

DOI: 10.1007/s11661-011-0911-9

© The Minerals, Metals & Materials Society and ASM International 2011

I. INTRODUCTION

THERE is a continuing interest in increasing the strength of steels without compromising formability or weldability. Bainitic steels are increasingly seen as promising candidates. The bainite transformation occurs between the temperatures of pearlite and athermal martensite formation in plain carbon and low alloy steels. Bainitic ferrite is frequently classified as upper or lower, depending on whether carbide formation has occurred at the ferrite-austenite interfaces or within the bainitic ferrite laths. Increasing the amount of silicon suppresses the development of carbides in these steels such that their final microstructures are mixtures of ferrite and retained austenite, often termed “carbide-free bainite.”* In this regard, the work of Bhadeshia and

*This term is in current use within the metallurgical community; it refers to a structure that is similar to true bainite, but which contains no carbides.

co-workers^[1,2] has elucidated the range of desirable properties that can be obtained from dispersions of ferrite and retained austenite.

Electrical resistivity measurement is a well-established method of continuously tracking phase transformations in steels;^[3] it provides information very similar to that obtained through other volume-averaging methods, such as dilatometry and magnetic saturation techniques.

I.A. YAKUBTSOV, formerly Research Associate, with the Department of Materials Science and Engineering, McMaster University, is now R&D Scientist, with the Integrity Testing Laboratory Inc., Toronto, ON, Canada. Contact e-mail: iyakubtsov@yahoo.com
G.R. PURDY, University Professor, is with the Department of Materials Science and Engineering, McMaster University, Hamilton, ON, Canada L8S 4L7.

Manuscript submitted January 13, 2011.

Article published online September 30, 2011

A significant acceleration of the onset of austenite decomposition occurs at temperatures just above the athermal martensite-start temperature M_S (for hypereutectoid compositions) and immediately below M_S in hypoeutectoid steels.^[4–10] This anomalous kinetic behavior was termed a “swing-back” phenomenon. The fast onset of the bainite reaction in hypoeutectoid steels below M_S was considered due to the effect of martensite plates on the nucleation of bainite in adjacent regions of untransformed austenite.^[4] Swing-back phenomena were elucidated by means of the study of the formation of lower bainite and isothermal martensite in hypereutectoid steels.^[11] The acceleration of reaction kinetics of lower bainite in medium carbon steel near the M_S temperature was attributed to stress created by the growth of lower bainite stimulating the formation of martensite and *vice versa*.^[12]

The idea has been advanced that austenite decomposition in plain carbon low alloy steels can be described as a continuum of bainitic ferrite and lath martensite formation in the appropriate temperature range.^[13] With decreasing temperature, thermodynamic conditions may develop that are conducive to the stimulation of martensite formation in residual austenite by growing bainitic laths because of an accommodation shear strain^[14] at temperatures just above M_S . In such a case, the martensite is not athermal.

The potential for the reduction of B_S via alloying provides for the refinement of bainitic laths and, as result, significantly enhances the strength of the final microstructure. Therefore, the bainite transformations at temperatures near M_S can create the multiphase mixtures of fine bainitic ferrite laths, retained austenite, and lath martensite in the final microstructures. The optimum combination of the volume fraction of each of them can form the final microstructures with superior strength and ductility. The lower B_S is also beneficial for the reduction of the cost of thermomechanical treatments for a given production line. Hence, the deep

understanding of the decomposition of austenite at the temperatures close to the M_S is important from both fundamental and applied points of views.

Despite intensive research on bainite transformation, very few systematic experimental studies were performed on the isothermal transformation kinetics of bainite in plain carbon and low alloy steels.^[15–22] Most of these dealt with the kinetics of either upper or lower bainites, both of which are influenced by precipitation of carbide phases. The first attempt to perform the comprehensive investigation of the overall kinetics of the formation of carbide-free bainite was due to Bhadeshia,^[17] who used dilatometric analysis. His experimental data were described by the classical Johnson–Mehl–Avrami–Kolmogorov (JMAK) approach, which held only up to a fraction transformed of about 0.6. The reaction constant n , as evaluated in this work, had a significant scatter and did not have a unique value, which could describe all experimental data. In a second study, isothermal bainite formation below the athermal M_S in a low alloyed steel C60 with 0.66 wt pct C was observed by dilatometry.^[21] The isothermal transformation studies were conducted in the temperature interval 573 K to 493 K (300 °C to 220 °C). M_S was about 537 K (264 °C). Microstructural observation by scanning electron microscopy revealed no carbide precipitation in the bainitic ferrite. Detailed analysis of the dilatometry data indicated that, following the formation of athermal martensite below M_S , the austenite continued to decompose isothermally with a rate corresponding to the kinetics of the bainite formation above M_S . The authors mentioned nothing about the possible formation of nonathermal martensite, which can accompany bainite transformation below M_S . The reaction constant n , transformation rate k , and apparent activation energy of bainite transformation were evaluated by the JMAK approach for this material as well.

The kinetics of austenite decomposition at the temperatures close to the M_S , where there exists a mutual (and, perhaps, synergistic) formation of bainitic ferrite and martensite, is an important fundamental topic in need of more detailed study. Information about kinetic parameters, and especially overall transformation rates at these temperatures, is particularly valuable from an engineering point of view, facilitating the design of appropriate thermotreatments for plain carbon and low alloy steels.

The objectives of this article are then to analyze the transformation kinetics of carbide-free bainite and to evaluate the kinetic parameters of the austenite decomposition such as a reaction constant n , rate constant $k = k(T)$, and apparent activation energy Q for transformations below and above M_S .

II. EXPERIMENTAL PROCEDURES

Material was prepared as a single melt. The cast was forged to bars with a cross section 50 × 50 mm, and then cut and homogenized for 5 days (120 hours) at 1623 K (1350 °C). The chemical composition of the experimental steel is presented in Table I. It is similar to

Table I. Chemical Composition Of Steel (Mass Percent)

C	Mn	Si	P	Ti	Al	Fe
0.40	2.78	1.81	0.009	0.004	0.004	balance

the composition first explored by Bhadeshia and Edmonds.^[1]

The study of the isothermal bainite transformation was performed by an electrical resistivity technique. The four-point method was used to measure the potential drop across the samples. The samples had dimensions of about 2 × 2 × 60 mm. The potential and current leads were spot-welded to a sample, and the measurements of potential drops were performed by reversing the known current flowing through the circuit. The samples were heated in an Argon protective atmosphere. The temperature of a sample was measured with the accuracy ±1 K (1 °C) by a K thermocouple attached to the sample. The setup (a quartz tube, probe with a sample, and thermocouple) was held in the furnace at the austenization temperature. It was taken out from the first furnace and air cooled. The constant monitoring of the temperature of the sample during air cooling provided the opportunity to put the sample inside the second furnace at the desired temperature for isothermal bainite transformation. Due to the hardenability of the alloy and size of the sample, the cooling rate of the sample in air was sufficient to ensure an isothermal transformation. Electrical resistances (ERs) of the samples were obtained from the measured potential and known current. The detailed description of the technique is given in Reference 23. The ER data presented in this work are normalized to the resistance of the samples at the beginning of the temperature for isothermal bainite transformation. The advantage of this approach is that size effects are avoided. Additionally, it allows the determination of the relative change of resistivity with temperature without requiring the measurement of the resistance of each sample. Good repeatability (about 99.5 pct) of ER behavior was found when measurements were repeated under the same experimental conditions.

The microstructural evolution in this alloy was observed on bulk samples 10 × 10 × 5 mm, which underwent conditions closely similar to those used in the ER experiments. The samples were held in argon atmosphere in a quartz tube. A thermocouple was located close to the sample inside the quartz tube. The setup was initially located in a furnace at austenization temperature. The entire setup was then removed from the furnace and air cooled to the temperature selected for isothermal transformation; it was then placed in a second furnace at that temperature, held for various times, and water quenched. Mechanically polished samples were etched in 2 pct Nital solution for observation by optical microscopy (OM). Microstructures were also characterized by transmission electron microscopy (TEM). Three-millimeter discs were cut from thin slices taken parallel to the metallographic sections. The discs were thinned in a Tenupol 3 electropolishing system (Struers Inc., Denmark) at 25 to 30 V and room temperature.

The volume fractions V_γ of austenite and its lattice parameters in the bulk samples were measured by XRD² (X-ray diffraction) technique using a Rigaku RU200 rotating anode diffractometer (Rigaku Americas Corp., The Woodlands, TX) with a cross-coupled parallel focusing mirror and Cu K_α radiation. The data were acquired with a Bruker SMART 6000 CCD detector on a D8 three circle goniometer, SMART, GADDS, TOPAS 2.1 software (Bruker Axs Inc., Madison, WI). The data collection and XRD² processing were performed by SMART and GADDS software. The phase composition is obtained by TOPAS 2.1 software.^[24] The volume fraction was taken as the average of three measurements for each sample, and the accuracy of its measurement is about ± 0.5 pct.

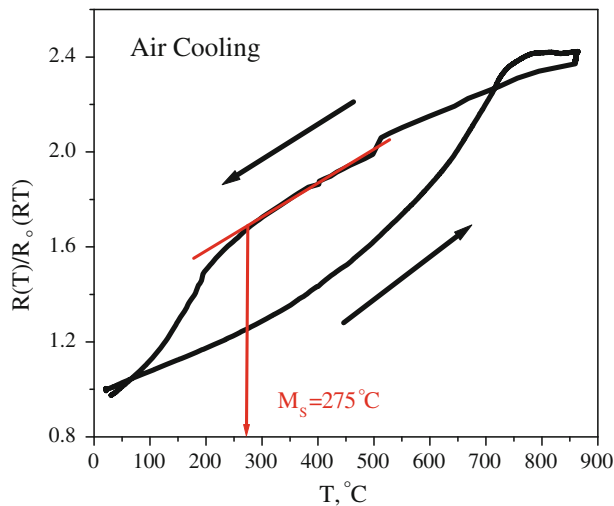


Fig. 1—Air cooling experiment for measurement of M_S (R_o (RT) is ER at room temperature).

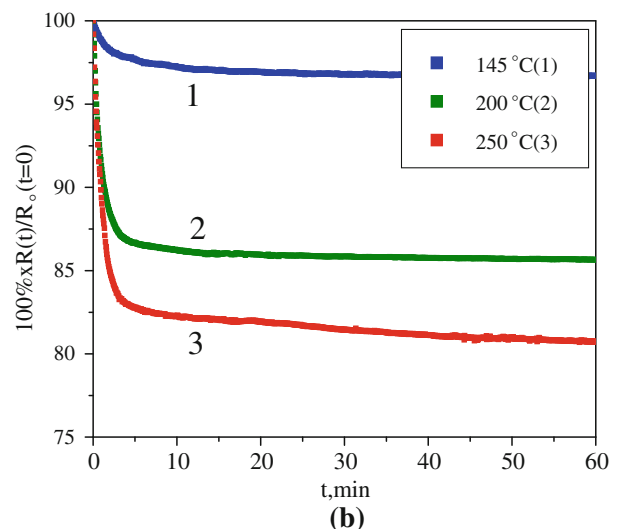
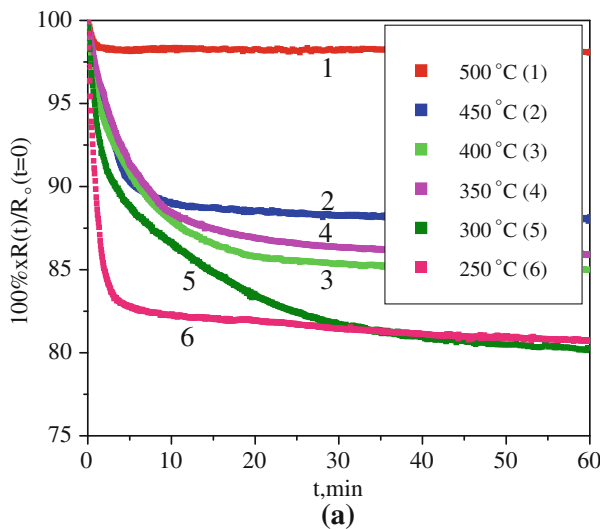


Fig. 2—Changes of ER vs time at different T_{IR} : (a) above and (b) below M_S .

III. RESULTS AND DISCUSSION

The athermal M_S for the steel under investigation was initially obtained by means of air cooling experiments. The sample was heated to 1133 K (860 °C) and held at this temperature for 1800 seconds; then, it was air cooled. Because this is an air-hardening composition, the deflection of a cooling path of ER was identified with the M_S . The behavior of ER during heating and air cooling is shown in Figure 1. The ER data at any temperature are normalized to the room-temperature ER R_o (RT). The experimental M_S is about 548 K (275 °C), which correlates well with the estimated M_S according to the empirical equation^[25]

$$M_S(^{\circ}\text{C}) = 539 - 423\text{C} - 30.4\text{Mn} - 12.1\text{Cr} - 7.5\text{Mo} - 7.5\text{Si} = 272^{\circ}\text{C} \quad [1]$$

where the symbol of each element corresponds to its composition in mass percent in solid solution of austenite.

Based on the experimental determination of M_S , a thermal processing schedule for the study of isothermal kinetics of bainite transformation was the following: the samples were held in the furnace for 1800 seconds at 1133 K (860 °C), allowed to cool to the desired isothermal reaction transformation temperatures T_{IR} , and the behaviors of their ER recorded.

The experimental behavior of ER during the first 60 minutes at the different T_{IR} values above and below M_S are presented in Figures 2(a) and (b), respectively. The numbers 1 through 6 of the curves in Figure 2(a) are in the order of the ER measurements at regularly spaced decreasing temperatures.

The changes of ER with time are associated with the isothermal decomposition of austenite at each temperature. The curves 1 and 5 in Figure 2(a) correspond to the highest 773 K (500 °C) and lowest 573 K (300 °C) temperatures of isothermal transformations above M_S . Curve 6 in Figure 2(a), which is presented for comparison,

shows the decomposition of austenite at the highest temperature 523 K (250 °C), just below M_S . The smallest and largest amounts of decomposition of austenite are observed at 773 K and 573 K (500 °C and 300 °C) above M_S , respectively. The fastest kinetics of the overall transformation is observed 573 K (300 °C); that is, about 25 K (25 °C) above M_S . Curve 6 in Figure 2(a), which represents the isothermal transformation approximately 25 K (25 °C) below M_S , shows a quite different profile of the decomposition of austenite compared to the other curves in Figure 2(a).

The results for austenite decomposition below M_S (at 523 K, 473 K, and 418 K (250 °C, 200 °C, and 145 °C)) are given in Figure 2(b). The magnitude of the ER change at the isothermal holding is scaled with the amount of the residual austenite left after the formation of athermal martensite during continuous cooling below M_S . The largest and smallest amounts of decomposition of austenite below M_S are at 523 K (250 °C) and 418 K (145 °C), respectively. The ER change at 418 K (145 °C) is quite small (curve 3, Figure 2(b)), because this temperature, most likely, is slightly above the athermal martensite finish temperature M_F . The profiles of the transformation kinetics are similar for all temperatures below M_S , and at the same time, they differ from the transformation kinetic profiles at the temperatures above M_S (curves 1 through 5 in Figure 2(a)).

The results of XRD measurements of the volume fractions V_γ of retained austenite, its lattice parameter a_γ , and the average carbon content C_{RA} in the bulk

Table II. XRD Measurements of Volume Fractions and Lattice Parameters of Austenite

T_{IR} [K (°C)]	V_γ (pct)	V_B (pct)	a_γ (nm)	C_{RA} (wt pct)
673 (400)	34	66	0.36095	0.95
573 (300)	25	75	0.36261	1.46

samples after isothermal holding at 673 K and 573 K (400 °C and 300 °C) for 2 hours are presented in Table II. The average carbon contents C_{RA} of the retained austenite were estimated according to the following expression:^[26]

$$C_{RA} = (a_\gamma \text{ (nm)} - 0.3578) / 0.0033 \quad [2]$$

The microstructural observations of bulk samples after holding at 673 K and 573 K (400 °C and 300 °C) were performed using OM (Figure 3) and TEM (Figure 4). The mean grain size of prior austenite was about 30 μm after austenization for 1800 seconds at 1133 K (860 °C). The final microstructure is a mixture of bainitic ferrite α_B and retained austenite (RA). The TEM study obtained that the retained austenite was observed between bainitic laths (Figures 4(a) and (b)) and at the boundaries of prior austenite (Figures 4(c) and (d)). The more detailed observation of microstructure at high magnification revealed that some islands of retained austenite have deformation microtwins (Figures 4(b) and (d)).

The fraction transformed Y at any temperature is a function of time t and can be expressed by the following expression:^[27]

$$Y(t) = \frac{R_o - R(t)}{R_o - R_f} = \frac{1 - \frac{R(t)}{R_o}}{1 - \frac{R_f}{R_o}} \quad [3]$$

where R_o is ER at the beginning of transformation, R_f is ER at the end of transformation, and $R(t)$ is ER at any time t .

The transformation kinetics of bainite transformation at different temperatures are presented in Figure 5. The fractions of transformed Y at different T_{IR} above and below M_S are presented in Figures 5(a) and (b), respectively. Figure 5(c) shows the evolution of bainitic ferrite and residual austenite with time at 673 K and 573 K

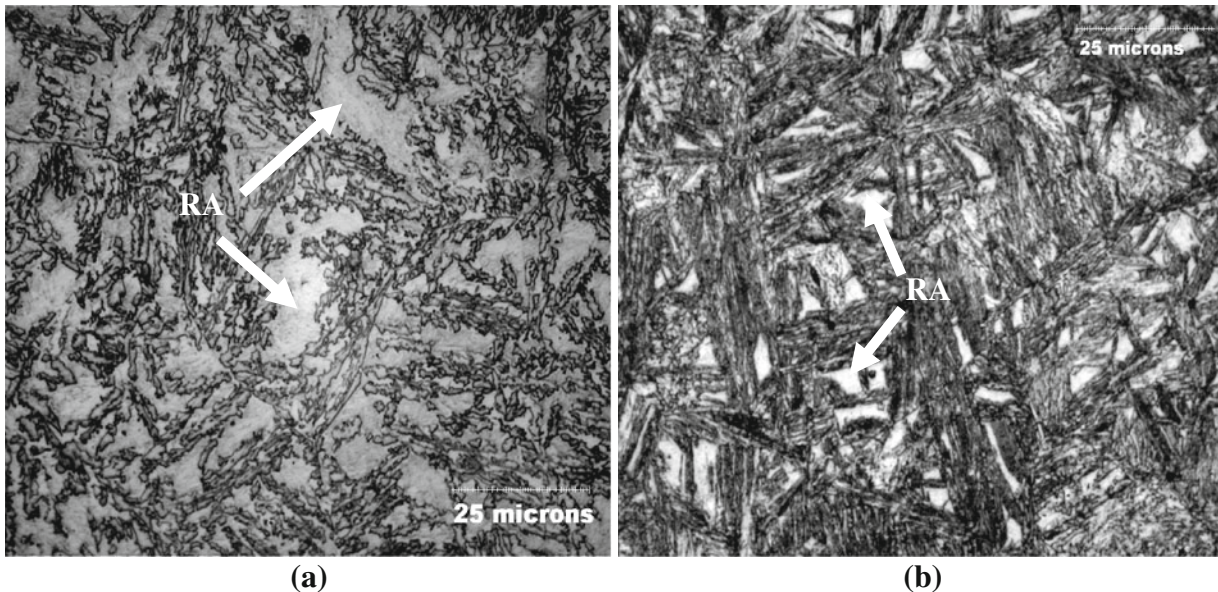


Fig. 3—Microstructures after holding for 2 h, OM: (a) 673 K (400 °C) and (b) 573 K (300 °C). RA is retained austenite.

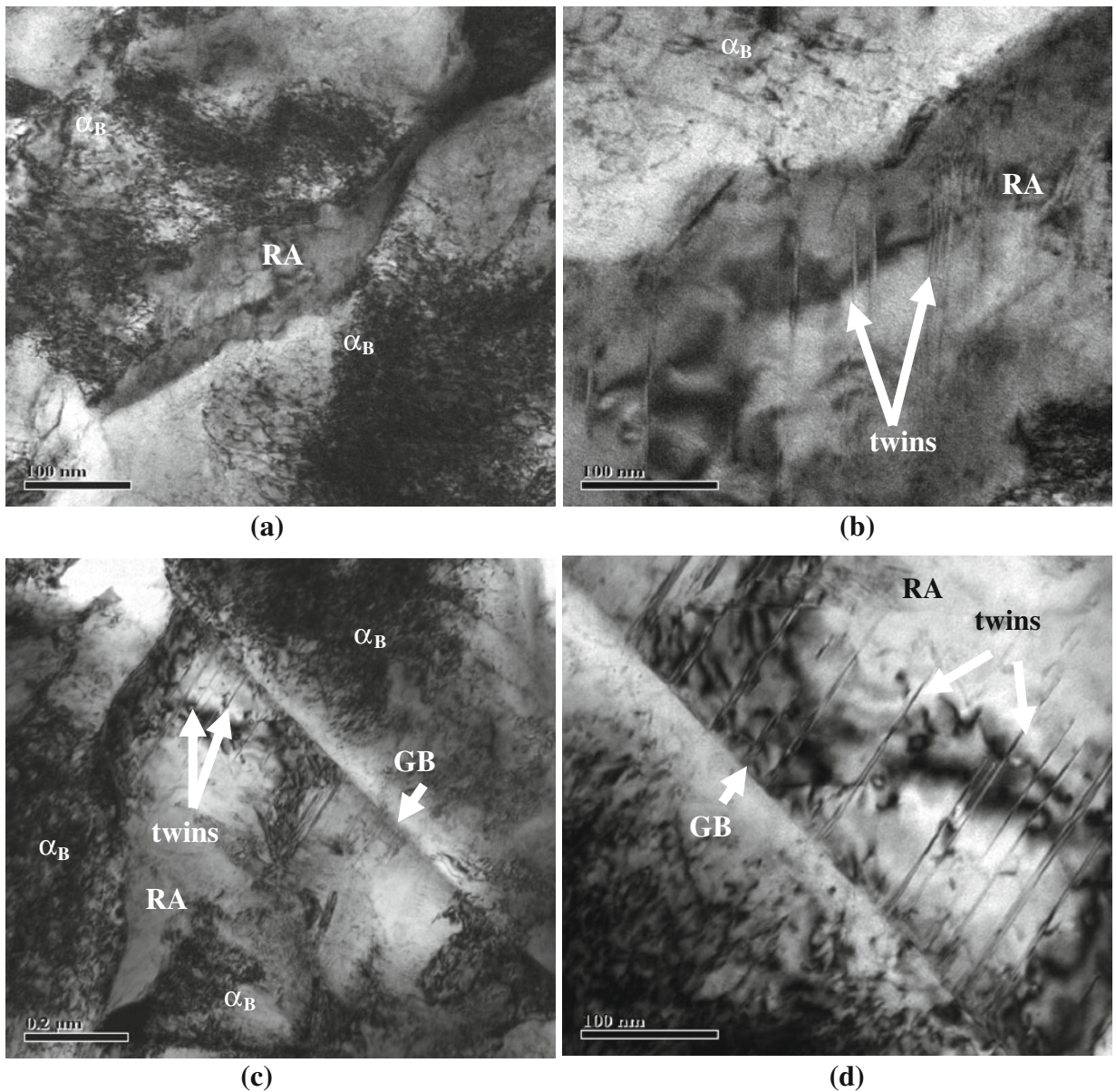


Fig. 4—Microstructures after holding for 2 h, TEM: (a) and (b) at 673 K (400 °C) and (c) and (d) at 573 K (300 °C). RA is retained austenite, α_B is bainitic ferrite, and GB is grain boundary of prior austenite.

(400 °C and 300 °C). The presented results in Figure 5(c) were received after the normalization of the ER data by the volume fractions of retained austenite obtained through the XRD measurements at the respective temperatures.

The analysis of transformation kinetics of bainite transformation was performed using the generalized kinetic equation,^[28] where an impingement parameter c was introduced. Like other kinetic models, the generalized kinetic equation is also a function of the kinetic parameters such as a rate constant $k = k(T)$ and reaction constant n , which depends on the nucleation mechanism and growth process. According to this procedure, the normalized transformed fraction Y changes with time t as

$$G(c) = \ln \left[\frac{(1 - Y)^{-c} - 1}{c} \right] = n \ln t + n \ln k \quad [4]$$

The correct value of the impingement parameter c results in the majority of the experimental data positioned on a straight line. The slope of this line gives n , and its interception with the y -axis obtains $n \ln(k(T))$. It should be emphasized that when $c = 0$, the generalized kinetic equation becomes equivalent to the JMAK equation,^[29–33] which is more appropriate for processes with hard impingement. The generalized kinetic equation corresponds to the Austin–Rickett (AR) dependence when $c = 1$,^[34] which depicts processes where soft impingement occurs; that is, the effect of concentration

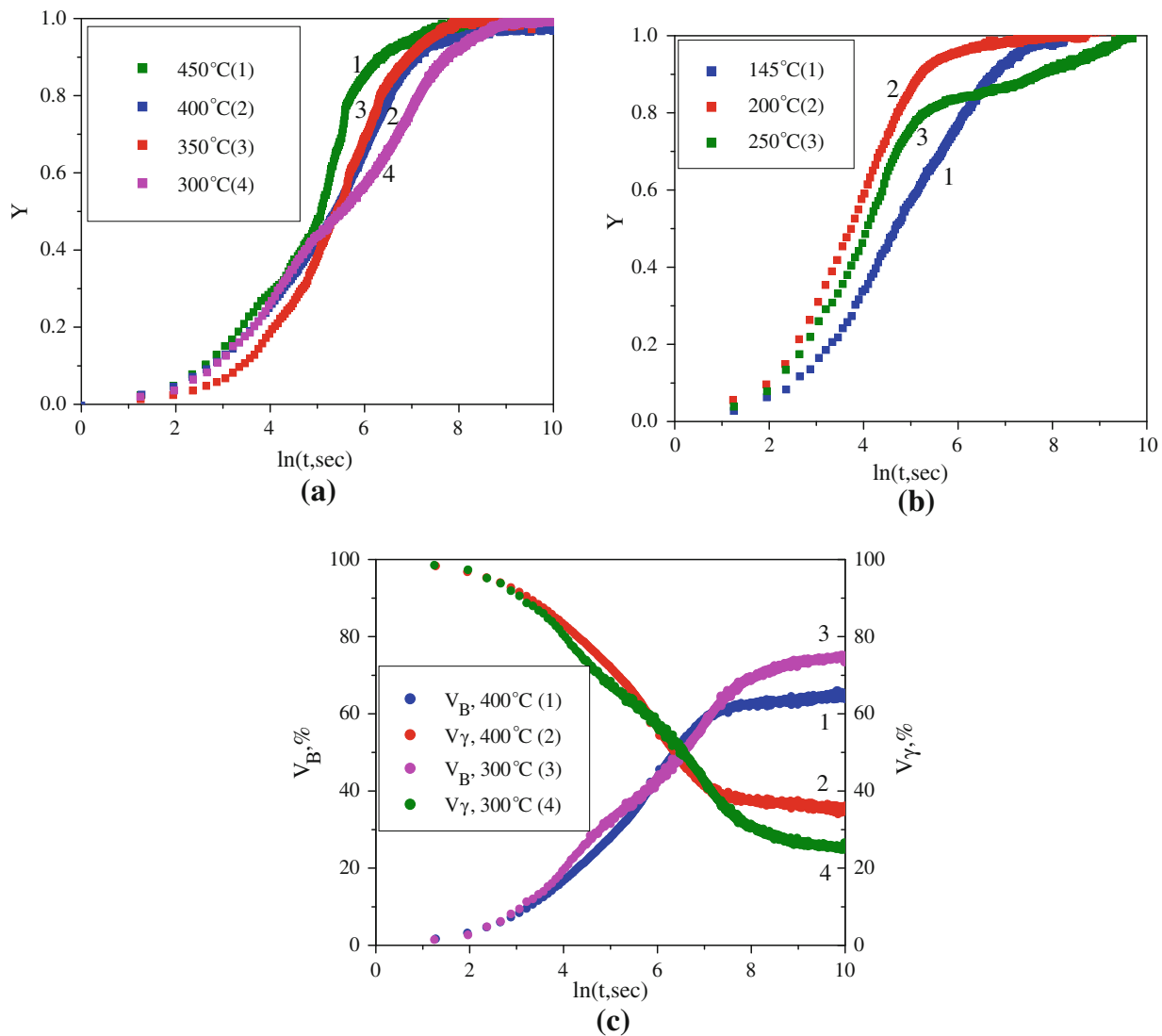


Fig. 5—Fractions transformed at T_{IR} (a) above and (b) below M_S . (c) Evolution of residual austenite and bainite at 673 K and 573 K (400 °C and 300 °C).

changes in the parent phase solid solution on precipitation (bainitic ferrite laths in our study). Therefore, Eq. [4] can be expressed as follows:

$$G(c) = \ln \left[\ln \left(\frac{1}{1-Y} \right) \right], c = 0, \text{JMAK} \quad [5a]$$

$$G(c) = \ln \left[\frac{Y}{1-Y} \right], c = 1, \text{AR} \quad [5b]$$

The examples of the functions $G(c)$ for the transformation kinetics at the different T_{IR} above and below M_S are presented in Figure 6. The analysis shows that the behavior of $G(c)$ is the same for both approaches approximately by the middle of the overall transformations ($Y \approx 0.5$ to 0.6), and their further behaviors become different at all temperatures T_{IR} . The $G(c)$ of

JMAK dependence illustrates the deviation from a linear relation with a negative curvature at some stage of transformation at any temperature T_{IR} . The $G(c)$ of the AR approach demonstrates more linear dependences for a longer time ($Y \approx 0.8$ to 0.9) during the transformations at all temperatures compared to the JMAK approach. The effect of the impingement parameter $c = 1$ on the behavior of $G(c)$ can be explained by carbon soft impingement through enrichment of residual austenite during bainite transformation. The AR dependence also has negative deviations from a linear relation at later stages of transformations at 573 K, 523 K, and 473 K (300 °C, 250 °C, and 200 °C). The minimum and maximum of the deviation are at 573 K and 523 K (300 °C and 250 °C), respectively (Figures 6(b) and (c)). The $G(c)$ of the AR approach, at the lowest $T_{IR} = 418$ K (145 °C), shows again a very close linear relation through essentially the whole transformation (Figure 6(d)).

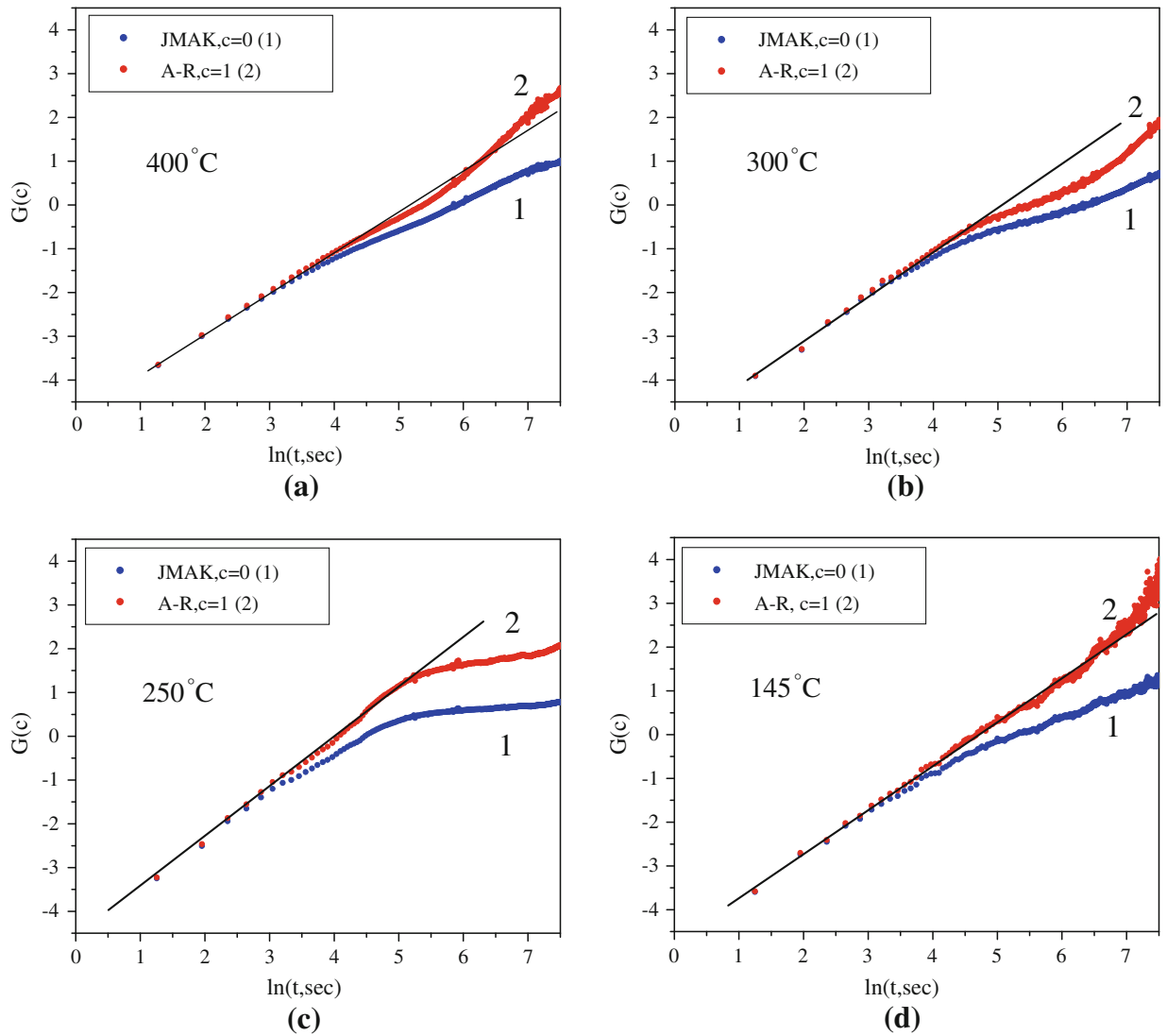


Fig. 6—Functions $G(c)$ for different T_{IR} above and below M_S : (a) 673 K (400 °C), (b) 573 K (300 °C), (c) 523 K (250 °C), and (d) 418 K (145 °C).

The weak correction of $G(c)$ by the impingement parameter confirms that the carbon impingement effect is not strong in the range 573 K to 473 K (300 °C to 200 °C), which covers the temperature interval from just above M_S to below M_S . The thermodynamic stability of the residual austenite is very low at these temperatures, and bainitic ferrite transformation can promote the formation of strain-induced martensite in adjacent residual austenite.^[35] The thermodynamic free-energy balance for the strain-induced martensite nucleation at T_{IR} in nondeformed residual austenite during bainite transformation is given by

$$\Delta G_{ch}^{\gamma \rightarrow \alpha} - \Delta G_{mech} + E_{nuc.str} + W_{fric} = 0 \quad [6]$$

where $\Delta G_{ch}^{\gamma \rightarrow \alpha}$ is the chemical driving force for the martensite formation in residual austenite and $\Delta G_{ch}^{\gamma \rightarrow \alpha} = G^\alpha - G^\gamma$ (G^α and G^γ are the molar Gibbs free energies for the bcc and fcc phases of the steel at T_{IR}); ΔG_{mech} is the additional mechanical driving force due to the strain of residual austenite in the areas adjacent to

bainitic ferrite and $\Delta G_{mech} = \sigma_\gamma \cdot M^{-1} \cdot S_\gamma \cdot V_m$; σ_γ is the flow stress of austenite at a true strain S_γ ; M is the Taylor factor for fcc polycrystals; V_m is the molar volume of the steel; $E_{nuc.str}$ is the strain energy accompanying nucleation for the martensite; and W_{fric} is the total interfacial friction work against martensite transformation in residual austenite, which is a function of solute atoms (carbon and other alloying elements) only in our case.^[36]

The formation of deformation microtwins in the residual austenite (which will have an increased stacking fault energy due to its increased carbon content) (Figure 4) confirms the development of strains at the temperatures 673 K and 573 K (400 °C and 300 °C) in the residual austenite, and it is consistent with other experimental data.^[37] Most likely, there is a nonuniform distribution of carbon in residual austenite at 573 K (300 °C) such that a comparatively minor amount of residual austenite with low carbon enrichment can be transformed to martensite by the developed strains.

The behavior of ER at this temperature (curve 5 in Figure 2(a) and curve 3 in Figure 2(b)) shows that the kinetics of decomposition of austenite is slightly different (faster) than at higher temperatures (curves 1 through 4 in Figure 2(a)). This effect is strongest at the temperature 523 K (250 °C), which is just below M_S , when there is the highest amount of metastable residual austenite. At this condition, bainite transformation forms the highest amount of strain-induced martensite, which has the strongest hard impingement effect on bainitic ferrite growth. This effect is less pronounced at the lower temperature of 473 K (200 °C) (curve 2 in Figure 2(b)), when the amount of residual austenite is lower after the formation of athermal martensite during continuous cooling to this temperature and a lower amount of strain-induced martensite forms, respectively, compared to 523 K (250 °C). The lowest amount of residual austenite at 418 K (145 °C) (curve 1 in Figure 2(b)) results in the lowest hard impingement effect due to strain-induced martensite, and soft carbon impingement influence is again strong enough at this temperature. The estimated values of the parameters n from the slope of the functions $G(c)$ for the AR dependences using Eq. [4] are presented in Figure 7(a), and they are very close to 1 at all temperatures B_S . The value $n = 1$ can be elucidated, according to Christian,^[38] as grain boundary nucleation after saturation with thickening of long needles (bainic ferrite laths in our case) after complete end impingement during growth. The experimentally obtained rate constant k shows the nonmonotonic behavior with the falling temperature B_S (Figure 7(b)); namely, k decreases in the temperature interval 723 K to 623 K (450 °C to 350 °C) with its following increase at 573 K (300 °C), and k is the highest at the temperatures 523 K and 473 K (250 °C and 200 °C) when the highest amounts of strain-induced martensite form during bainite transformation that effects the overall transformation rate of austenite decomposition. The further decrease of B_S to 418 K (145 °C) provides a decline of k to its approximate magnitude at 573 K (300 °C), which is associated

with a very low amount of thermodynamically metastable residual austenite at 418 K (145 °C). The transformation constant k of the austenite decomposition in the temperature interval 573 K to 418 K (300 °C to 145 °C) can be presented in the form $k = k_B + k_M$, where k_B and k_M are the transformation constants of bainite and martensite transformations, respectively. The transformation constant k of a very low amount of metastable austenite at 418 K (145 °C) is determined by a combination of a very low transformation rate of bainite k_B (solid line in Figure 8(b), see text below) and transformation rate of martensite k_M .

The apparent activation energy Q of isothermal austenite decomposition can be obtained by the following method:^[39]

$$-\ln(t_Y) = -\frac{Q(Y)}{RT} + \ln B(Y) \quad [7]$$

where t_Y is the time taken to transform a given amount of Y , $Q(Y)$ is an average activation energy corresponding

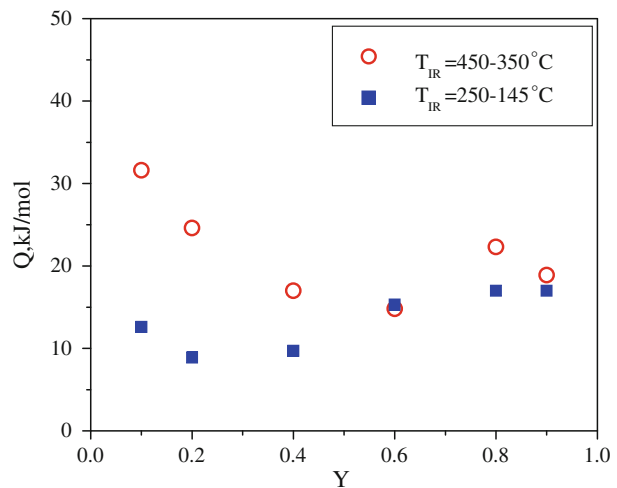


Fig. 8—Apparent activation energy Q at the different transformed amount Y for T_{IR} above and below M_S .

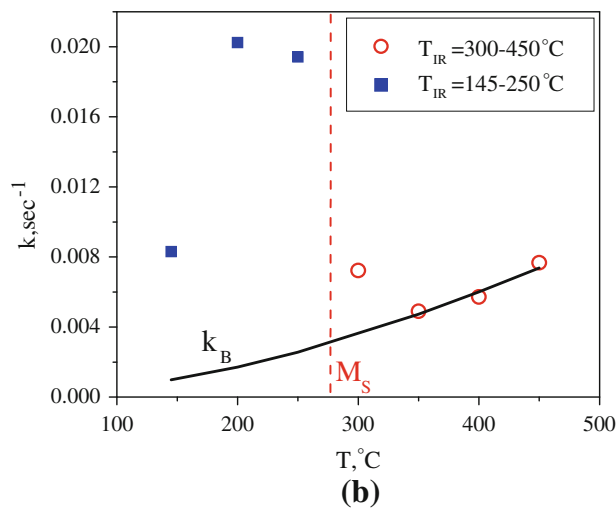
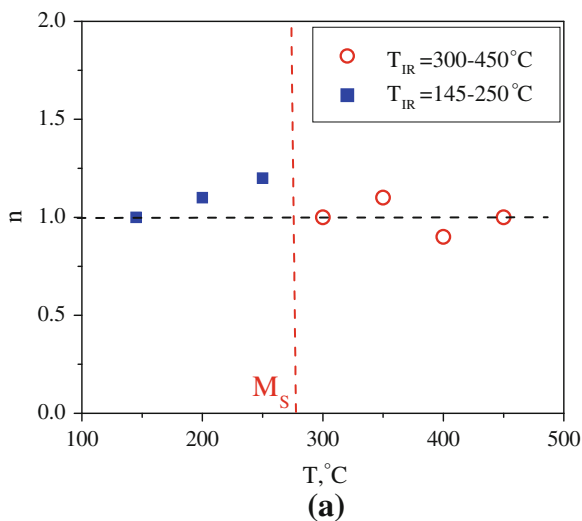


Fig. 7—(a) Reaction constant n and (b) rate constant k vs temperature (k_B is a rate constant only for bainite transformation).

to some mean value from $Y = 0$ to a given amount of Y , R is the universal gas constant, and T is the absolute temperature.

A plot of $-\ln(t_Y)$ vs $1/T$ gives a straight line with a slope of $-Q/R$. To estimate the average activation energy for only bainitic ferrite formation at the temperatures above M_S , the analysis was performed only for the temperature interval 723 K to 623 K (450 °C to 350 °C) to avoid any possible additional effect of strain-induced martensite at the $T_{IR} = 573$ K (300 °C) on the value of Q . The estimated activation energies after the linear regression vs the different transformed amounts Y are presented in Figure 8. There is a spread of activation energies through the progress of transformation according to the experimental data. Nevertheless, the apparent activation energies for austenite decomposition below and above M_S are about 13 and 22 kJ/mol, respectively. The analysis of the constant rate k_B for bainite transformation only in the temperature interval 723 K to 623 K (450 °C to 350 °C) using the Arrhenius equation $k_B = k_{Bo} \exp(-Q/RT) = 11.64 \cdot 10^{-2} \exp(-16,588.1/RT)$ has shown that the apparent activation energy Q of austenite decomposition is about 17 kJ/mol. Based on the two types of assessments, the activation energy for bainite transformation is about 20 kJ/mol in this study. The extrapolation of k_B below 623 K (350 °C) gives the information about the magnitude of the transformation rate of bainitic ferrite only below M_S (solid line in Figure 7(b)). The lower value of Q for austenite decomposition at the temperatures below M_S can be explained by a combined formation of bainitic ferrite and strain-induced martensite. The evaluation of Q , using the experimental data of the different techniques (metallography, electrical resistivity, and dilatometry), showed that apparent activation energy Q of isothermal bainite transformation in plain carbon and low alloy steels, which have different thermohistories and alloy chemistries, increases monotonically with the carbon contents in the range of about 0.1 to 1.2 wt pct C.^[15–21] The reported data of Q vary approximately from 10 to 60 kJ/mol for lower bainite and from 50 to 135 kJ/mol for upper bainite. That covers the activation energies for isothermal α -martensite transformation in high alloyed iron-based alloys ($Q_M = 1$ to 50 kJ/mol),^[40–44] diffusion of carbon in ferrite ($Q_C^f = 80$ kJ/mol),^[45] and close to carbon diffusion in austenite ($Q_C^a = 157$ kJ/mol).^[46] Despite the broad variety of Q for bainite transformation in the literature data, the presented evaluated apparent activation energies Q of bainite transformation above M_S and austenite decomposition by a combined formation of bainite and strain-induced martensite below M_S in the carbide-free steel are quite reasonable and are close to the range of the published values for the lower bainite and α -martensite in high alloyed iron-based materials.

IV. SUMMARY AND CONCLUSIONS

The alloy studied contained silicon sufficient to suppress a carbide formation; hence, the isothermal resistivity response primarily reflects the formation of bainitic ferrite. A recent analysis of the intrinsic resistivity

of austenite and ferrite has placed the subject on a firmer physical basis:^[47] it is suggested that the anomalously high resistivity of metastable austenite at lower temperatures is due to electron scattering by spin disorder. The source of the ER response is not of primary concern here, however. The large change in resistivity accompanying the precipitation of ferrite confers the benefit of sensitivity on the method, and the correlation of resistance change with martensite and bainite formation is found to be consistent and reproducible. We are then interested in the application of the method in the study of overall transformation kinetics, in particular, the evaluation and interpretation of the reaction constant n , the rate constant $k = k(T)$, and the apparent activation energy Q below and above the athermal martensite-start transformation temperature $M_S = 548$ K (275 °C).

The resulting reaction constant n is close to 1 for all temperatures of isothermal transformations, which would correspond in Christian's classification to site-saturated grain boundary nucleation, followed by lengthening of ferrite laths to complete end impingement, and their subsequent thickening.

The rate constant k exhibits a much more complex behavior with temperature over the range investigated, first decreasing from 723 K to 623 K (450 °C to 350 °C), then increasing with decreasing temperature to a maximum at about 523 to 473 K (250 to 200 °C), and falling again as the lowest temperature, 418 K (145 °C), is approached. This nonmonotonic behavior is thought to be related to the amount of strain-induced martensite accompanying the isothermal bainite transformation in the temperature interval 573 K to 418 K (300 °C to 145 °C), where the residual austenite is expected to possess a reduced thermodynamic stability. The amount of strain-induced martensite also probably influences the magnitude of the hard impingement effect for isothermal bainite transformation; this effect correlates with the amount of martensite formed in the temperature interval 573 K to 418 K (300 °C to 145 °C). Soft impingement of diffusion fields from nearby ferrite laths will result in the carbon enrichment (and consequent increased stability) of residual austenite, in the temperature interval 723 K to 623 K (450 °C to 350 °C), where only bainite transformation occurs.

The apparent activation energy Q for bainite transformation temperatures above M_S is higher than that below M_S , where martensite precedes (and presumably assists) bainite formation. The apparent activation energies Q obtained in this work are close to the range of the published values for the formation of lower bainites in plain carbon and low alloy steels and α -martensites in highly alloyed iron-based materials.

We conclude that the measurement of ER is an effective method of following the formation of carbide-free bainitic ferrite, yielding information comparable to (and sometimes superior to) that obtained with dilatometric and other volume-averaging methods. In this special case of carbide-free bainites, one can draw certain inferences concerning the synergy between the martensite and bainite reactions, while discriminating between the athermal and isothermal processes.

In the present work, we find overall consistency with a model comprising a site-saturated nucleation stage, an initial growth (lengthening) process, and a final thickening of bainitic ferrite laths, accompanied by carbon enrichment and (consequent) increased stability of the retained austenite. It is considered highly probable that the processes of bainite and martensite formation are able to catalyze one another.

ACKNOWLEDGMENTS

This research was supported by the Natural Sciences and Engineering Research Council of Canada. The authors are grateful to Drs. M. Niewczas and J. Britten for access to the ER equipment and for the XRD measurements, respectively.

REFERENCES

- H.K.D.H. Bhadeshia and D.V. Edmonds: *Met. Sci.*, 1983, vol. 17, pp. 411–20.
- F.G. Caballero and H.K.D.H. Bhadeshia: *Curr. Opin. Solid State Mater. Sci.*, 2004, vol. 8, pp. 251–57.
- O.N. Mohanaty and A.N. Bhagat: *Mat.-wiss. Werkstofftech.*, 2003, vol. 34, pp. 96–101.
- S.V. Radcliffe and E.C. Rollason: *J. Iron Steel Inst.*, 1959, vol. 191, pp. 56–65.
- P.W. Brown and D. Mack: *Metall. Trans.*, 1973, vol. 4, pp. 2639–43.
- O. Schaaber: *Trans. AIME*, 1955, vol. 203, pp. 559–60.
- R.T. Howard and M. Cohen: *Trans. AIME*, 1949, vol. 176, pp. 384–97.
- M.F. Smith, G.R. Speich, and M. Cohen: *Trans. TMS AIME*, 1959, vol. 215, pp. 528–30.
- N.F. Kennon and R.T. Edwards: *J. Aust. Inst. Met.*, 1970, vol. 15, pp. 195–200.
- T.Z. Wozniak: *Mater. Charact.*, 2008, vol. 59, pp. 708–16.
- M. Oka and H. Okamoto: *Metall. Trans. A*, 1985, vol. 19A, pp. 447–52.
- L.C. Chang: *Mater. Sci. Eng.*, 2004, vol. A368, pp. 175–82.
- G.R. Purdy and M. Hillert: *Acta Metall.*, 1984, vol. 32, pp. 823–28.
- H.K.D.H. Bhadeshia and D.V. Edmonds: *Metall. Trans. A*, 1979, vol. 10A, pp. 895–907.
- G.R. Speich and M. Cohen: *Trans. TMS-AIME*, 1960, vol. 218, pp. 1050–59.
- M.J. Hawkins and J. Barford: *Scripta Mater.*, 1970, vol. 4, pp. 583–88.
- H.K.D.H. Bhadeshia: *J. Phys.*, 1982, Coll. C4, Suppl. 12, pp. C4-443–C4-448.
- M. Umemo, K.H. Uchi, and I. Tamura: *Trans. ISIJ*, 1982, vol. 22, pp. 854–61.
- D. Quidort and Y.J.M. Brechet: *ISIJ Int.*, 2002, vol. 42 (9), pp. 1010–17.
- J.W. Elmer, T.A. Palmer, S.S. Babu, W. Zhang, and T. DebRoy: *Weld. J.*, 2004, Sept., pp. 244–53.
- S.M.C. van Bohemen, M.J. Santofimia, and J. Sietsma: *Scripta Mater.*, 2008, vol. 58, pp. 488–91.
- N.V. Luzginova, L. Zhao, and J. Sietsma: *Mater. Sci. Eng.*, 2008, vols. A481–482, pp. 766–69.
- M. Niewczas, Z.S. Basinski, S.J. Basinski, and J.D. Embury: *Phil. Mag.*, 2001, vol. 81A, pp. 1121–38.
- General Area Detector Diffraction System (GADDS), Version 4.0, User's Manual*, Bruker AXS Inc., Madison, WI, 1999.
- K.W. Andrews: *JISI*, 1965, vol. 203, pp. 721–27.
- D.J. Dyson and B. Holmes: *JISI*, 1970, vol. 208, pp. 469–74.
- I.S. Servi and D. Turnbull: *Acta Metall.*, 1966, vol. 14, pp. 161–69.
- E.-S. Lee and Y.G. Kim: *Acta Metall. Mater.*, 1990, vol. 38, pp. 1669–76.
- W.A. Johnson and K.E. Mehl: *Trans. Am. Inst. Min. Met. Enf.*, 1939, vol. 195, pp. 416–58.
- M. Avrami: *J. Chem. Phys.*, 1941, vol. 9, pp. 177–84.
- M. Avrami: *J. Chem. Phys.*, 1939, vol. 7, pp. 1103–12.
- M. Avrami: *J. Chem. Phys.*, 1940, vol. 8, pp. 212–24.
- A.N. Kolgomorov: *Izv. Akad. Nauk SSSR, Ser. Mater.*, 1937, vol. 1, pp. 355–59.
- J.B. Austin and R.L. Rickett: *Trans. Am. Inst. Eng.*, 1939, vol. 135, pp. 396–415.
- G.B. Olson and M. Cohen: *J. Less-Common Met.*, 1972, vol. 28, pp. 107–18.
- G. Ghosh and G.B. Olson: *Acta Metall. Mater.*, 1994, vol. 42, pp. 3361–70.
- E. Swallow and H.K.D.H. Bhadeshia: *Mater. Sci. Technol.*, 1996, vol. 12, pp. 121–25.
- J.W. Christian: *Theory of Phase Transformation in Metals and Alloys*, Pergamon Press, Oxford, United Kingdom, 2004, pp. 529–46.
- M. Hillert: *Acta Metall.*, 1959, vol. 7, pp. 653–58.
- G.V. Kurdjumov and O.P. Maksimova: *Dokl. Akad. Nauk SSSR*, 1948, vol. 61, pp. 83–93.
- G.V. Kurdjumov and O.P. Maksimova: *Dokl. Akad. Nauk SSSR*, 1950, vol. 73, pp. 95–98.
- S.R. Pati and M. Cohen: *Acta Metall.*, 1971, vol. 19, pp. 1327–32.
- C.T. Peters, P. Bolton, and A.P. Miodownik: *Acta Metall.*, 1972, vol. 20, pp. 881–86.
- S.K. Gupta and V. Raghavan: *Acta Metall.*, 1975, vol. 23, pp. 1239–45.
- C. Wells, W. Barz, and R.F. Mehl: *Trans. AIME*, 1950, vol. 188, pp. 553–60.
- H. Sueyoshi and K. Suenaga: *J. Jpn. Inst. Met.*, 1987, vol. 51, pp. 518–24.
- U. Bohnenkamp, R. Sandstrom, and G. Grimvall: *J. Appl. Phys.*, 2002, vol. 92, pp. 4402–07.